HC	hydrocarbon
W	water

Registry No. Benzene, 71-43-2; hexane, 110-54-3; cyclohexane, 110-82-7; ethanol, 64-17-5; methanol, 67-56-1.

Literature Cited

(1) Arbuckle, W. B. *Environ. Sci. Technol.* **1983**, *17*, 537-542.
(2) Arbuckle, W. B. *Environ. Sci. Technol.* **1986**, *20*, 1060-1064.
(3) Yalkowsky, S. H.; Roseman, T. J. In *Techniques of Solubilization of Drugs*; Yalkowsky, S. H., Ed., Marcel Dekker: New York, 1981.
(4) Bannerjee, S. *Environ. Sci. Technol.* **1984**, *18*, 587-591.
(5) Munz, C.; Roberts, P. V. *Environ. Sci. Technol.* **1986**, *20*, 830-836.
(6) Holmes, M. J.; Van Winkle, M. *Ind. Eng. Chem.* **1970**, *62*, 21-31.
(7) Polak, J.; Lu, B. C. Y. *Can. J. Chem.* **1973**, *51*, 4018-4023.
(8) Price, L. C. *AAPG Bull.* **1976**, *20*, 213-244.
(9) Varteressian, K. A.; Fenske, M. R. *Ind. Eng. Chem.* **1936**, *28*, 928.
(10) Groves, F. R. *Environ. Sci. Technol.* **1988**, *22*, 282-286.
(11) Chang, Y. C.; Moulton, R. W. *Ind. Eng. Chem.* **1953**, *45*, 2350.
(12) Mertslin, R. V.; Kamaevskaya, L. A.; Nikurashina, N. I. *Zh. Fiz. Khim.* **1966**, *40*, 2539.
(13) Ross, S.; Patterson, R. E. *J. Chem. Eng. Data* **1979**, *24*, 111.
(14) El-Zoobi, M. The Effect of Alcohols on the Solubility of Hydrocarbons in Water. M.S. Thesis, Louisiana State University, 1989.
(15) Prausnitz, J. M.; Anderson, T.; Grens, E.; Eckert, C.; Hsieh, R.; O'Connell, J. *Computer Calculations for Multicomponent Vapor-Liquid and Liquid-Liquid Equilibria*; Prentice-Hall: Englewood Cliffs, NJ, 1980.
(16) Anderson, T. F.; Prausnitz, J. M. *Ind. Eng. Chem. Process Des. Dev.* **1978**, *17*, 552-561.

Received for review April 3, 1989. Accepted April 29, 1990. This work was supported by the Louisiana State University Hazardous Waste Research Center via a grant from the U.S. Environmental Protection Agency. However, it does not necessarily reflect the views of the Agency and no official endorsement should be inferred.

Three-Dimensional Simulation of Radon Transport into Houses with Basements under Constant Negative Pressure

Celso O. Loureiro* and Linda M. Abriola

Environmental Engineering Program, Department of Civil Engineering, The University of Michigan, Ann Arbor, Michigan 48109

James E. Martin

Environmental and Industrial Health, School of Public Health, The University of Michigan, Ann Arbor, Michigan 48107

Richard G. Sextro

Indoor Air Quality Program, Lawrence Berkeley Laboratory, University of California, Berkeley, California 94720

■ A theoretical evaluation of the properties and processes affecting the transport of radon into houses with basements is presented. A three-dimensional finite-difference model is developed to simulate the following: (1) the production and decay of ^{222}Rn in the soil; (2) the diffusive and convective transport of ^{222}Rn within the soil; (3) the entry of ^{222}Rn into the house through idealized openings in the understructure of the building; and (4) the final indoor ^{222}Rn activity concentration, computed as a function of a negative pressure applied in the basement of the house. The basic assumptions of the model include steady-state conditions, a rigid soil matrix, constant soil moisture, and a homogeneous distribution of properties within defined soil regions. Illustrative simulations are presented for dry soil conditions. A sensitivity analysis reveals that the most significant variables for the establishment of the indoor ^{222}Rn concentration are the ^{226}Ra concentration in the soil particles, the soil permeability, and the applied pressure difference. The relative importance of diffusive and convective mechanisms is explored for parameter ranges of interest.

Introduction

Under normal operating conditions, residential buildings can generate small pressure differences across the subgrade portion of the building shell. These pressure differences, when negative, may induce a flow of soil gas from the subsurface into the interior of the house through openings in the understructure. Radon gas produced in the soil can, thus, be transported into the house by molecular diffusion and gas-phase convection. In this process, the building acts as a trap for radon. Depending upon the radon entry rate and the building air exchange rate, the indoor radon can reach concentrations typically 1 order of magnitude larger (but possibly ranging far higher) than concentrations in the outdoor ambient air (*1*, *2*). Although other sources of indoor radon, such as building materials, groundwater utilization, and natural gas may be significant in some specific cases, the most important source of high indoor radon concentrations in single-family houses in the United States appears to be the soil gas surrounding the building foundations (*3*, *4*).

Radon is a radioactive noble gas, which decays in a sequence of short-lived decay products. When inhaled, these airborne short-lived radon progeny attach to the internal walls of the respiratory tract, exposing the lung tissues to damaging α radiation. Exposure to radon daughters has been associated with the induction of lung cancer in miners, mostly in the uranium mining industry (*5-8*).

The objective of this article is to present a theoretical evaluation of soil- and house-related factors affecting the transport of radon from the soil into houses. A three-dimensional finite-difference mathematical model is developed to simulate the processes associated with the following: (1) radon production and decay in the soil around the house; (2) the diffusive and convective transport of radon within the soil; (3) radon entry into the house through idealized openings in the understructure of the building; and (4) the final indoor radon activity concen-

 0013-936X/90/0924-1338$02.50/0

tration, computed as a function of a negative pressure applied in the basement of the house.

Early interest in radon transport processes below the earth's surface centered on applications involving environmental conditions and open soil only, with no consideration of the effect of a built structure (a house for instance) on the soil surface (*9*, *10*). Mathematical models associated with these applications may be found in refs 11–17. Models expressing the transport of radon into houses and the resultant indoor radon concentration are still at an early stage of development and are not very numerous. In initial modeling efforts it was assumed that the dominant transport mechanism was the diffusion of radon from building materials (*18*). Later, the importance of pressure-driven flow and the generation of radon in the soil were recognized (*19–21*).

Analytical and numerical solutions of a simplified transport equation (neglecting diffusion) for radon entrance into houses employing highly simplified geometries have been described in (*22–24*). Analytical solution of the complete set of equations governing the transport of radon into houses through openings in the building shell is not feasible, even for simple geometries. A few numerical solutions have been presented for simplified two- (*25–27*) and three-dimensional (*28*) domains. These models, however, neglect the diffusive mechanism of radon transport within the soil. In 1987, the United States Department of Energy, Office of Health and Environmental Research, increased the support for basic scientific research on radon, expanding its ongoing Radon Research Program. New projects were designed to determine the availability and transport of radon in the environment and to model the transport of radon within the soil and into buildings (*29*). Some of the modeling projects conducted under this program have already been concluded (*24*, *30–32*). A few others are still in progress, with only preliminary descriptions available (*33–35*).

The radon transport model presented in this article constitutes an important first-generation step in the modeling effort to characterize the production and transport of radon in soil and its entrance into houses. A detailed description of the model is presented in ref 30. In contrast to most existing modeling approaches, the model incorporates both diffusive and convective transport processes. It can be used to simulate the final indoor radon activity concentration as a function of the underpressure in the house and also computes the three-dimensional distribution of the disturbance pressure, soil gas velocity, and radon activity concentration in the soil gas. Although the model can accommodate small and constant soil moisture content (below field capacity), the calculations presented here are exclusively related to dry soils. This model is unique in its application to radon migration and entry into houses and provides the basic theoretical framework for further investigation of this phenomenon.

Conceptualization of the Physical Model

The model is based on a single-family house with poured concrete basement floor and walls. A gap is assumed to exist at the junction between the floor and the walls along the perimeter of the basement, as a result of building design or from the natural shrinkage of the concrete basement floor slab. This gap is assumed to be the only opening in the understructure of the house and consequently, the only communicating channel available for the soil gas flow. Radon diffusion through the concrete of the floor and walls is assumed to be negligible. The soil is presumed to be the only source of indoor radon. Although the house would actually be composed of a number of separate levels, it is treated, for the calculation of indoor radon mixing, as a single chamber (*21*, *23*). The soil block around the understructure of the house is considered to be an unsaturated porous medium with no open channels and fractures and to consist of well-defined regions of homogeneous and isotropic materials. In order to fully account for the effects of spatial variation of parameters affecting radon entrance into the house, the model is fully three-dimensional. Constant moisture content of the soil can be treated in a parameterized approach, during the selection of values for the input parameters of the model. In this approach, the choice of input parameters is made initially for moisture content level, according to correction criteria discussed elsewhere (*21*, *30*). The simulations presented in this article are exclusively related to dry soils.

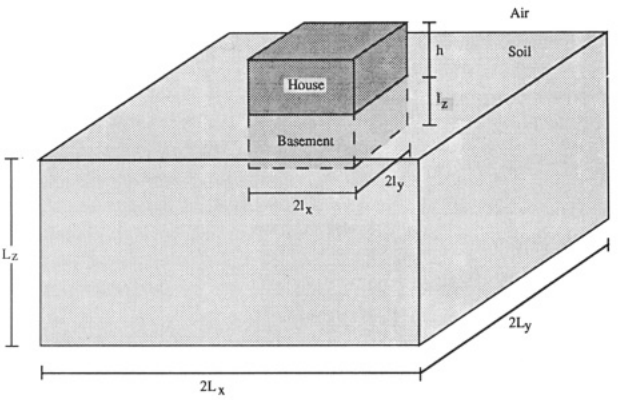

Figure 1. Geometric configuration adopted in the model. The large rectangular parallelepiped represents the soil. The house is represented by the smaller parallelepiped, with the basement embedded in the center and upper part of the soil block.

The major assumptions adopted for the development of the mathematical model are the following: (1) the subsurface system is composed of three isothermal phases—solid soil, water, and gas; (2) the soil phase behaves as a rigid matrix; (3) there is no moisture migration within the system; (4) steady-state conditions prevail for the pressure and radon transport equations; (5) within each defined region in the soil, the soil properties are isotropic and homogeneous; (6) the soil gas phase is composed of a mixture of atmospheric air with a relatively small molecular concentration of radon; (7) the soil gas density is unaffected by the molecular concentration of radon and does not change appreciably over the expected range of pressure variability. Other assumptions and simplifications are described below.

The geometric configuration of the model is shown in Figure 1. The soil block under consideration is represented as a rectangular parallelepiped of dimensions $2L_x$, $2L_y$, and L_z. The house is treated as a smaller rectangular parallelepiped of dimensions $2l_x$, $2l_y$, and $(l_z + h)$, partially embedded in the center and upper part of the soil block. The basement, represented by the part of the house embedded in the soil block has the dimensions $2l_x$, $2l_y$, and l_z. A region of aggregate soil material, in which the soil properties can be altered from those of the undisturbed soil block, is located around the basement. Its thickness is represented by l_{ax}, l_{ay}, and l_{az} in the x, y, and z directions, respectively. Due to symmetry in the xy plane, the model was developed for a reduced geometric configuration shown in Figure 2. The entry route for soil gas into the basement is defined as the concrete shrinkage gap located at the wall–floor joint along the perimeter of the basement floor. This gap is idealized as an opening bounded by two parallel plates (the floor slab and the wall). The gap width is defined by the separation between the floor slab and the

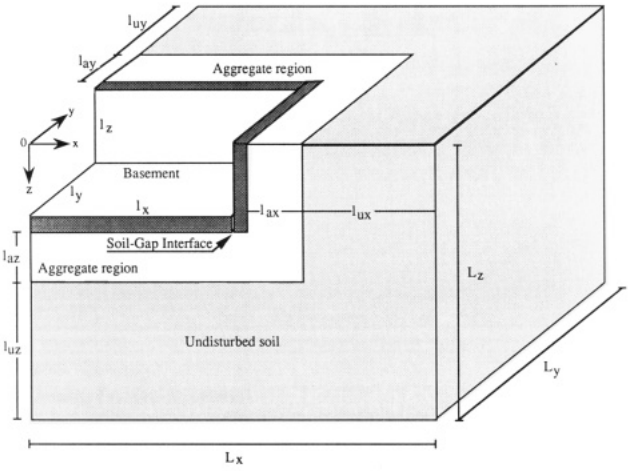

Figure 2. Quarter of the soil block where the numerical solution for the model is developed.

wall, and its depth by the thickness of the floor slab.

The important conceptual features of the model, and the interdependence of its elements, are shown schematically in Figure 3. The sequence of events begins with a negative pressure disturbance, Δp, generated inside the house as a result of wind effect, heating, and unbalanced mechanical ventilation. This disturbance pressure is added to the absolute pressure in the basement, at the defined gap, and propagates through the soil, establishing a steady pressure distribution. The newly established disturbance pressure distribution then induces a steady nonuniform flow of soil gas through the soil matrix. Radon generation, radioactive decay, and diffusive transport are coupled with convective flow (as expressed by the radon mass transport equation) to establish the flux density of radon activity through the soil and the radon entry rate into the house. Finally, based on radon entry rate, house dimensions, and ventilation rate, the resultant indoor radon activity concentration is computed.

Development of the Mathematical Model

Equation Development. The mathematical model describing the generation and transport of radon in the soil consists of two coupled equations: a flow equation, expressing the disturbance pressure distribution; and a transport equation, expressing the distribution of the radon activity concentration in the gas phase, throughout the soil. To develop these equations one may begin with the general mass balance equation for a given species i in a phase j. Here, a species i is defined as a specific chemical component such as radon or a group of components with some average characteristics such as water, soil air, and soil particles. A phase j can be any phase present in the subsurface system: the soil (s), water (w), or gas (g) phase. The general mass balance equation can be written as (*36*)

$$\frac{\partial(\epsilon_j \rho_j \omega_{ij})}{\partial t} = \vec{\nabla}\cdot(\epsilon_j \rho_j \vec{\vec{D}}_{ij}\cdot\vec{\nabla}\omega_{ij}) - \vec{\nabla}\cdot(\rho_j \omega_{ij}\vec{q}_j) + R_{ij} + S_{ij} \quad (1a)$$

subject to the following constraints

$$\sum_j \epsilon_j = 1 \quad (1b)$$

$$\sum_i \omega_{ij} = 1 \quad (1c)$$

$$\sum_j S_{ij} = 0 \quad (1d)$$

where (all variables will be described in their order of appearance) ϵ_j is the volume fraction of phase j; ρ_j is the mass density of phase j (kg m^{-3}); ω_{ij} is the mass fraction of component i in phase j; $\vec{\vec{D}}_{ij}$ is the macroscopic second-order tensor representing the effective dispersion coefficient of component i in phase j (m^2 s^{-1}); $\vec{q}_j$ is the relative superficial velocity vector of phase j (m s^{-1}); R_{ij} is the external source, or sink, of component i in the phase j (kg m^{-3} s^{-1}); and S_{ij} is the interphase transfer source/sink term (kg m^{-3} s^{-1}). Summing eq 1a over all components i of a phase j generates a continuity equation for phase j. Because the soil matrix has been assumed rigid and the water phase immobile, only the gas-phase continuity equation need be considered herein. If one neglects the contribution of radon to the total soil gas mass and employs constraint 1c, the mass balance equation for the soil gas phase becomes

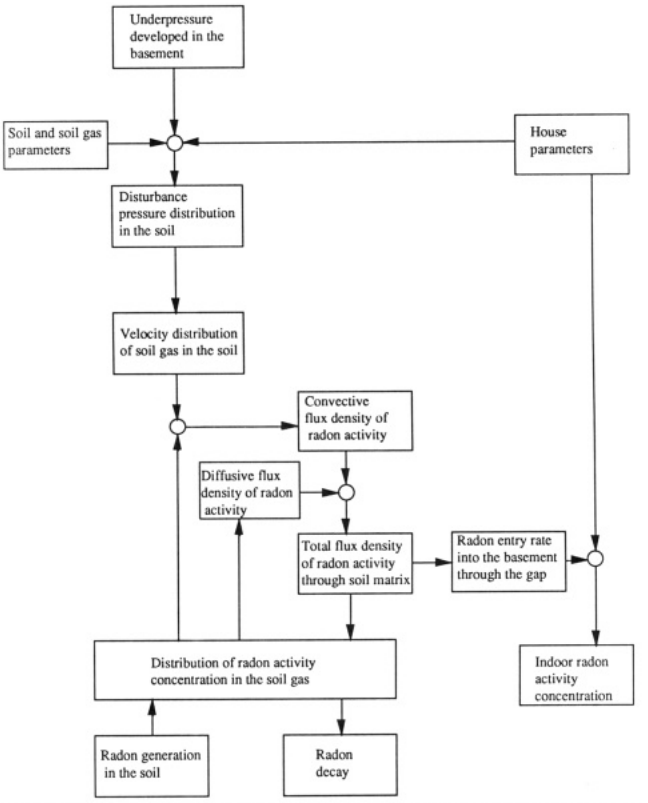

Figure 3. General flow chart representing the main elements of the radon transport model.

$$\frac{\partial(\epsilon_g \rho_g)}{\partial t} + \vec{\nabla}\cdot(\rho_g \vec{q}_g) = 0 \quad (2)$$

Note that the dispersive terms sum to zero over a phase. Because the amount of radon present in the soil gas is at the molecular level, and the expected range of pressure variation in the soil is very small (a few pascals), the soil gas will be considered incompressible. Thus, under steady-state conditions, the continuity equation for the soil gas phase becomes

$$\vec{\nabla}\cdot\vec{q}_g = 0 \quad (3)$$

An equation for the disturbance pressure field in the soil can be derived by coupling eq 3 with the expression for soil gas velocity given by Darcy's law. For isotropic soils, the differential form of Darcy's law for soil gas phase flow is (*37*)

$$\vec{q}_g = -\left(\frac{k k_{rg}}{\mu_g}\right)(\vec{\nabla}P_g - \rho_g \vec{g}) \quad (4)$$

where k is the intrinsic permeability of the soil matrix (m^2);

k_{rg} is the relative permeability of the soil gas phase; μ_g is the soil gas dynamic viscosity (N s m^{-2}); P_g is the absolute pressure of the soil gas phase (N m^{-2}); and $\vec{g}$ is the gravity acceleration vector (m s^{-2}).

In the modeled system, the absolute pressure distribution in the soil gas phase is the sum of two independent pressure components: the hydrostatic pressure and the "disturbance pressure". This disturbance pressure distribution results from the application of a pressure disturbance at the gap. The resultant absolute pressure P_g, then, is given as

$$P_g = P_A + \rho g z + p_g \tag{5}$$

where P_A is the atmospheric pressure (absolute pressure at depth $z = 0$) (N m^{-2}); and p_g is the disturbance pressure in the soil gas phase (N m^{-2}). Incorporating eqs 4 and 5 into eq 3 yields

$$\vec{\nabla}\cdot(k k_{rg}\vec{\nabla}p_g) = 0 \tag{6}$$

where it has been assumed that the soil gas viscosity does not vary appreciably in space. Variation of air viscosity with temperature in the range of 20 ± 10 °C is less than ±5% (*38*). Equation 6 is a linear second-order partial differential equation describing the disturbance pressure field distribution in the soil matrix. For the model presented herein, the intrinsic soil permeability for the soil gas phase, $k_g = k k_{rg}$, is assumed to be block-wise constant within specified regions of the soil. In general, k_g is dependent on the moisture content in the soil, since k_{rg} is a function of water saturation (*21*).

The general mass balance equation (eq 1) may be summed over the gas and water phases to yield a radon mass balance expression:

$$\frac{\partial(\epsilon_g C_g + \epsilon_w C_w)}{\partial t} = -\vec{\nabla}\cdot\vec{J}_g + (R_g + R_w)\left(\frac{\lambda N_A}{M_{Rn}}\right) + (S_g + S_w)\left(\frac{\lambda N_A}{M_{Rn}}\right) \tag{7a}$$

where, here, a radon activity/mass conversion factor ($\lambda N_A/M_{Rn}$) has been employed and the radon diffusion in the water phase has been neglected. The variables C_g and C_w are the radon activity concentrations in the soil gas and water phases, respectively, (Bq m^{-3}); $\vec{J}_g$ is the bulk flux density of radon activity through the soil matrix (Bq m^{-2} s^{-1}); R_g and R_w represent the rate of decrease of radon mass within the gas and water phases, respectively, due to radioactive decay (kg m^{-3} s^{-1}); S_g and S_w represent the net radon mass interphase transfer into the gas and water phases, respectively, (kg m^{-3} s^{-1}); λ is the radon radioactive decay constant (s^{-1}); N_A is Avagadro's number; and, M_{Rn} is a kilomole of radon. The radon activity concentrations in the gas and water phases may be related by the Henry's law:

$$C_w = K_H C_g \tag{7b}$$

where K_H is the coefficient of solubility of radon in water. The bulk flux density of radon activity in the soil, $\vec{J}_g$, is made up of two components: the convective ($\vec{J}_{gC}$) and diffusive ($\vec{J}_{gD}$) radon activity flux densities. For an isotropic soil, with a constant soil gas density (not affected by the presence of radon), it can be expressed as

$$\vec{J}_g = \vec{q}_g C_g - \epsilon_g D_e \vec{\nabla} C_g \tag{8}$$

where D_e is the effective diffusion coefficient of radon in the gaseous phase of the soil matrix (m^2 s^{-1}). Since the velocity of the soil gas is expected to be very small throughout the soil (except at the regions very close to the soil–gap interface), the mechanical dispersion of radon is not expected to be significant and, consequently, has been neglected.

The sum of the radon mass interphase transfer terms multiplied by the radon activity/mass conversion factor is equal to the net amount of radon activity that is generated within the solid phase and escapes into the soil pore space, per unit of total volume and time. It can be expressed as (*21*)

$$(S_g + S_w)\frac{\lambda N_A}{M_{Rn}} = nG = (n) f \rho_s C_{Ra} \lambda\left(\frac{1-n}{n}\right) \tag{9}$$

where G is the production rate of radon activity into the soil pore space (Bq m^{-3} s^{-1}), f is the radon emanating fraction, ρ_s is the density of the soil grains (kg m^{-3}), C_{Ra} is the concentration of radium activity in the soil particles (Bq kg^{-1}), and n is the porosity of the soil matrix.

The variation of radon activity due to radioactive decay within the gas and water phases, per unit of total volume and time, can be expressed as

$$(R_g + R_w)\frac{\lambda N_A}{M_{Rn}} = -\lambda(\epsilon_g C_g + \epsilon_w C_w) \tag{10}$$

Substituting eqs 3 and 8–10 into eq 7 results in the general radon transport equation for the subsurface system. Under steady-state conditions, this becomes

$$\vec{\nabla}\cdot(\epsilon_g D_e \vec{\nabla} C_g) - \vec{q}_g\cdot\vec{\nabla} C_g - \lambda(\epsilon_g + K_H \epsilon_w) C_g + f \rho_s C_{Ra} \lambda (1-n) = 0 \tag{11a}$$

where D_e, f, and $\vec{q}_g$ (or k_{rg}) are functions of the water saturation (*21*). For a dry soil, ($\epsilon_w = 0$ and $\epsilon_g = n$), the equation reduces to

$$\vec{\nabla}\cdot(D\vec{\nabla} C_g) - \vec{q}_g\cdot\vec{\nabla} C_g - \lambda n C_g + f \rho_s C_{Ra} \lambda (1-n) = 0 \tag{11b}$$

where $D = nD_e$ is the bulk diffusion coefficient of radon in the soil matrix. Solution of eq 11a or eq 11b provides the radon activity concentration field, in the gas phase, throughout the soil. The simulations presented in this article are based on the solution of eq 11b. Calculations related to soils with constant and small moisture content can also be performed with the model by solving eq 11a. In this case then, the input parameters D_e, f, and k_{rg} must be evaluated as functions of ϵ_w.

Boundary Conditions. There are five distinct boundaries in the soil block shown in Figure 2 at which conditions must be specified to solve the flow and transport equations. These boundaries are (1) the soil–air interface, (2) the soil–gap interface, (3) the soil–wall and soil–floor interfaces, (4) the external (bottom and lateral) sides of the soil block, and (5) the internal sides (symmetry surfaces). At the top of the soil block (soil–air interface), first type boundary conditions are specified. There, the absolute pressure is equal to the atmospheric pressure, and according to eq 5, the disturbance pressure in the soil gas phase (p_g) is equal to zero. Since the concentration of radon in the atmospheric air [typical values of 4.0 Bq m^{-3} (*7*)] is much smaller than C_g [typical values of 2.0 × 10^4 Bq m^{-3} (*30*)] and since it is expected that air will flow from the atmosphere into the ground, driven by the negative disturbance pressure field, it is assumed that C_g is negligibly small (zero) at the soil–air interface.

The boundary conditions at the interface between the gap and the soil underneath it required careful consideration. There, the major difficulty is that the boundary values of the variables (either p_g or C_g) are unknown and, therefore, have to be calculated iteratively. To solve the problem, the concept of continuity is imposed for flow and

transport within the crack. During the iterations, the soil gas velocity and the radon activity flux density through the gap are calculated separately, considering the region of the gap as a distinct domain (separated from the soil block domain). Analytical solutions for the soil gas velocity and the radon activity flux density throughout the gap region are employed to express the values of those variables as functions of their respective values at the soil–gap interface. Further details of this gap treatment can be found in ref 30. If the soil gas velocity and the radon activity flux density within the gap domain are known, the principle of continuity along with a first type boundary condition can then be applied at the soil–gap interface. According to the continuity principle it is assumed that, for example, in the case of the flow equation, p_g and the vertical component of $\vec{q}_g$ at the interface are both continuous functions of space. Radon activity concentration and flux density are treated similarly, in the solution of the transport equation.

The other regions illustrated in Figure 2 are treated as no-flow boundaries. The effective radon diffusion coefficient and the intrinsic permeability of concrete (walls and floor) are much smaller than their respective values in the soil, and consequently from eqs 4 and 8, both $\vec{q}_g$ and $\vec{J}_g$ perpendicular to those structures are assumed to be zero. The bottom and lateral sides of the soil block are assumed to be located at a sufficiently large distance from the gap such that the disturbance pressure and radon concentration fields are essentially invariant with distance. Therefore, $\vec{q}_g$ and $\vec{J}_g$ perpendicular to those surfaces are also assumed to be zero. This assumption was supported by simulations to ensure that the size of the domain did not significantly affect the computed results (*30*). Finally, the internal surfaces of the soil block are treated as no-flow boundaries due to symmetry.

Indoor Radon Activity Concentration. Solution of the coupled flow and transport equations provides the flux density of radon activity throughout the calculation domain, including the gap region. The total entry rate of radon activity into the house, E_{total}, can then be evaluated as the product of the radon activity flux density at the exit of the gap into the house and the average cross-sectional area of the gap. Finally, based on a mass balance within the house, the indoor radon activity concentration can be calculated:

$$\frac{dC_{indoor}}{dt} = \frac{E_{total}}{V} - (\lambda + \lambda_V)C_{indoor} + \lambda_V C_{outdoor} \quad (12)$$

where C_{indoor} is the indoor radon activity concentration (Bq m^{-3}); $C_{outdoor}$ is the outdoor radon activity concentration (Bq m^{-3}); V is the total volume of the house (m^3); and, λ_V is the air exchange rate (ventilation rate) (s^{-1}). At steady state, and neglecting the outdoor radon contribution, C_{indoor} can be expressed as

$$C_{indoor} = \frac{E_{total}}{V(\lambda + \lambda_V)} \quad (13)$$

Computer Model. The equations representing the disturbance pressure and the radon activity concentration fields in the soil block are linear, three-dimensional, second-order partial differential equations which, together with the imposed boundary conditions, were solved numerically by using a Patankar–Spalding finite-difference numerical technique (*30*, *39–41*). In this approach, the solution domain is divided into nonoverlapping control volumes, with a node or a grid point defined at the center of each control volume. The governing partial differential equation is then integrated over each control volume. Piecewise interpolation functions expressing the spatial profile of the dependent variable between grid points are defined in order to evaluate the integral properly. The result of this discretization approach is a set of algebraic equations, one for each grid node, expressing the value of the dependent variable as a function of the values at a group of neighbor nodes. The attractiveness of the control-volume approach in deriving the discretized equations is that it guarantees the conservation of the physical quantities over any group of control volumes and, consequently, over the whole calculation domain. This feature is independent of the grid mesh size, and even a coarse grid mesh solution would present an exact integral balance (*40*).

An alternating direction iterative algorithm was adopted for the solution of the very large system of algebraic equations obtained from the application of the numerical method. In this iterative method, the three-dimensional grid is solved line by line, as well as layer by layer, in an alternating-direction sequence. At each iteration, the system is reduced to the equations representing only one line of nodes, which is solved by the Thomas algorithm (*40*). The process is repeated until the values of the unknown variable converge to a finite distribution throughout the calculation domain, including the soil–gap interface. Convergence was determined by examination of normalized changes in the unknowns with an adopted tolerance criterion of 10^{-4}. This alternating direction method was validated by solving a two-dimensional heat-transfer problem of simple geometry. Model results compared very well with the analytical solution. The method was shown to be efficient in the present application, resulting in fast and stable convergence of the unknown variables to a finite distribution under many diverse circumstances (*30*).

The computer model implementing the numerical method described above was designed as an interactive code composed of two coupled main programs named PRESSU and MASTRA (*30*), which are run separately. The first specifies the geometric parameters of the model, generates the control volumes and the computational grid, calculates the p_g and $\vec{q}_g$ distributions, and stores the simulated results in permanent files. In the second program, these results along with additional input parameters are used to calculate the distribution of C_g throughout the soil block. The radon flow through the gap and into the basement is also computed along with the resultant indoor concentration. Important input parameters to the model are given in Tables I and II.

Modeling Results

A hypothetical house located in a dry soil environment, with an air exchange rate of 1.0 h^{-1}, was used as a base case for the analysis of the model. Other specifications of this base case house are presented in Table I. Some of the parameter values adopted for the base case (the calculation domain and the numerical grid) were selected during the adjustment of the computer model and were shown to satisfy the boundary conditions imposed at the external surfaces of the block reasonably well (*30*). The behavior of the model, based on some convenient measures characterizing specific aspects of the process, will be described below. These measures are the values of $\vec{q}_g$, C_g, and $\vec{J}_g$ at the soil–gap interface, averaged over the whole extent of the gap. An understanding of the variation of these measures and their dependence on the house- and soil-related variables becomes helpful in explaining the total entrance of radon into the house and the resultant variation of indoor radon activity concentration. Table II presents a list of the variables selected for the simulations, with their typical values and expected range of variability.

Table I. Parameters Defined for the Base Case of the Model

parameter	value	unit	remark
house dimensions			
basement slab, $2l_x \times 2l_y$	10.0 × 15.0	m × m	
basement height, l_z	2.0	m	
height of the house, h	3.0	m	
thickness of the walls, l_w	0.15	m	$l_{wx} = l_{wy} = l_{wz}$
soil block dimensions			
aggregate region, l_a	0.5	m	$l_{ax} = l_{ay} = l_{az}$
undisturbed layer, l_u	10.0	m	$l_{ux} = l_{uy} = l_{uz}$
final calculation domain	15.65 × 18.15 × 12.65	m × m × m	(x, y, z) directions
numerical grid	27 × 29 × 27	no. of nodes	(x, y, z) directions, varying space

Table II. Range and Typical Values of the Input Parameters Used for the Simulations

parameter	typical value	range	unit	ref
C_{Ra}	40.0	10.0–200.0	Bq kg^{-1}	21
f	0.2	0.05–0.7		21
ρ_s	2.65×10^3	$(2.6–2.8) \times 10^3$	kg m^{-3}	21
Δp	5.0	0.0–20.0	Pa	27
w	1.0×10^{-3}	$(0.5–10.0) \times 10^{-3}$	m	30
k	1.0×10^{-12}	10^{-14}–10^{-9}	m^2	21
D	1.0×10^{-6}	$(0.5–5.0) \times 10^{-6}$	m^2 s^{-1}	21
n	0.5	0.4–0.6		21

The sensitivity of modeling results to each of the variables is explored below.

Radon Source Variables. The first three soil-related variables listed in Table II (^{226}Ra concentration in the soil particles, radon-emanating fraction, and soil particle density) are related exclusively to the production rate of radon into the soil pore space, G, as expressed in eq 9. Predictions of the model for the distribution of radon concentration in the soil, the radon entry rate into the house, and the indoor radon concentration can be shown to be directly proportional to G. Consequently, they are also directly proportional to those soil-related radon source variables. Therefore, because of its large range of variability, the concentration of ^{226}Ra in soil particles is clearly an important variable in the process of transporting radon from soil into houses.

Applied Disturbance Pressure Difference. Normalized distributions of the disturbance pressure field and the radon activity concentration in the soil gas, relative to the base case, in a vertical cross section of the soil block are shown in Figures 4 and 5, respectively. Here, the vertical cross section corresponds to a vertical cut in the xz plane located at the origin of the soil block (center of the house). The isolines in Figure 4 represent points of equal disturbance pressure, normalized to the interval (−1, 0), where −1 is the pressure at the basement, and 0 is the pressure at ground level outside. The isolines in Figure 5 represent points of equal radon activity concentration in the soil gas, C_g, normalized to the limit value of C_g^∞ at infinite depth in the soil.

Under steady-state conditions, the shape of the spatial distribution of the disturbance pressure throughout the soil block, as shown in Figure 4, is not affected by the value of the negative disturbance pressure applied at the basement. However, the absolute value of the pressure gradient at any point within the soil changes linearly with the applied disturbance pressure difference, Δp. Consequently, the seepage velocity of the soil gas through the soil $\vec{q}_g$ also changes linearly with Δp according to Darcy's law, as expressed in eq 4. On the other hand, under the same conditions, the shape of the spatial distribution of C_g/C_g^∞, as shown in Figure 5, is affected by the flow of soil gas and therefore depends on Δp. As the flow of soil gas toward

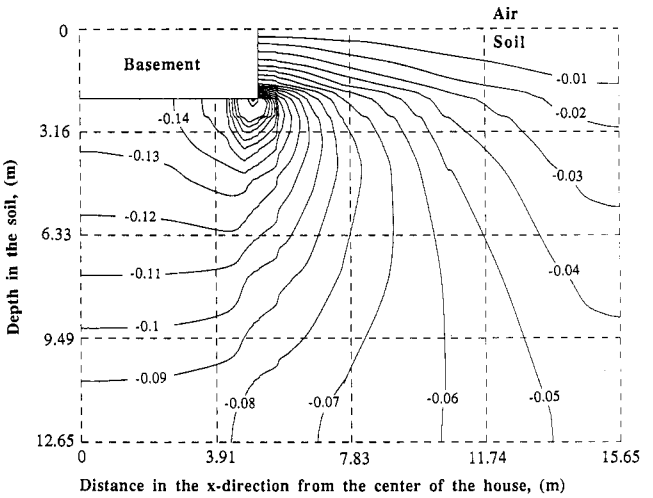

Figure 4. Normalized distribution of the disturbance pressure, p_g, in a vertical xz cross section of the soil block. The isolines represent the points of equal p_g, normalized to the value of the negative disturbance pressure difference, Δp, applied in the basement.

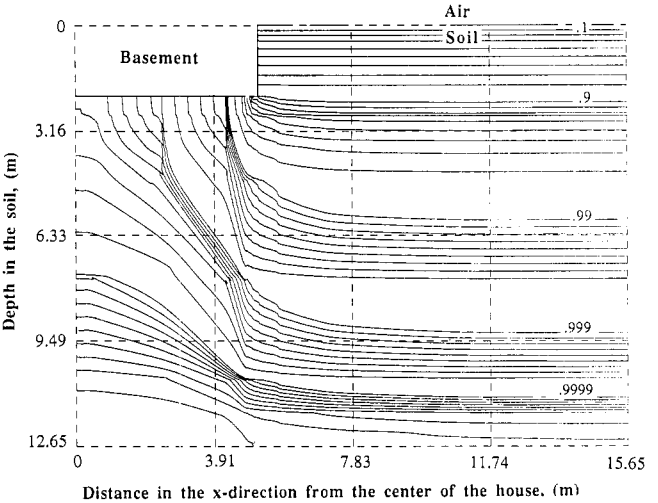

Figure 5. Normalized distribution of radon activity concentration in soil gas, C_g, in a vertical xz cross section of the soil block. The isolines represent the points of equal C_g, normalized to the finite limit value of radon activity concentration, C_g^∞, reached at infinite depth in the soil.

the gap is increased with an increase in Δp, the isolines in the C_g/C_g^∞ distribution at both the lower part of the soil block (soil gas richer in radon) and the upper part (radon-poor soil gas) move closer to the soil–gap interface. The overall value of C_g at the soil–gap interface will then either increase due to the contribution of radon-enriched soil gas from greater depth or be diluted by the contribution of radon-poor soil gas from the top of the soil block. The relative importance of this concentration–dilution effect depends on the distribution of the soil gas flow field throughout the soil block. In any case, the increase in $\vec{q}_g$,

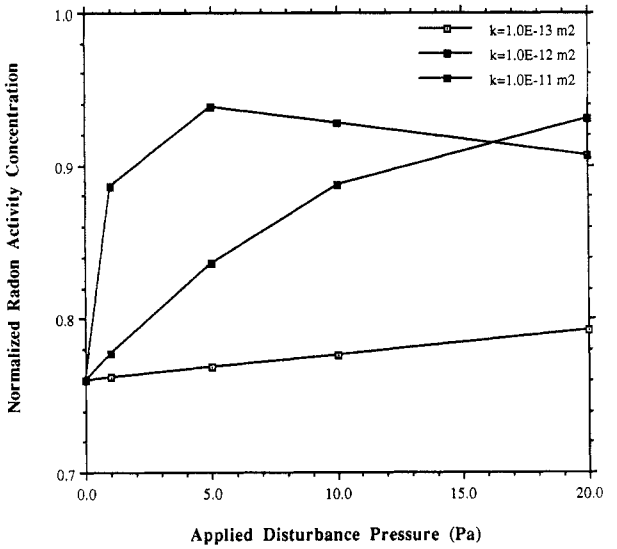

Figure 6. Normalized radon activity concentration in the soil gas, C_g/C_g^{∞}, averaged along the perimeter of the soil–gap interface, as a function of the applied disturbance pressure difference, Δp, for different values of soil permeability, k.

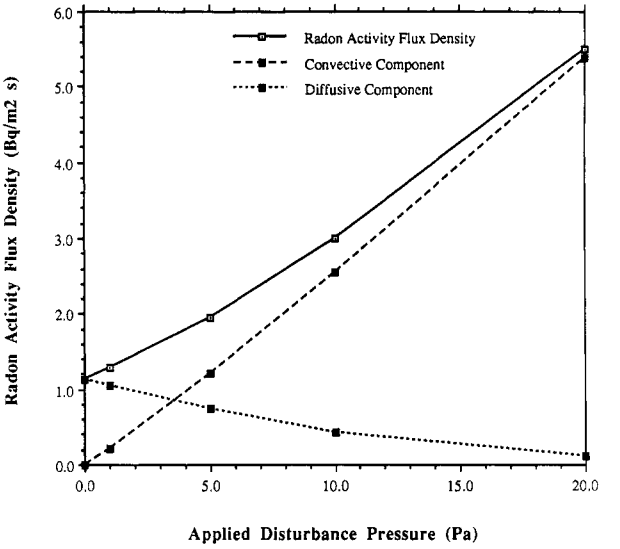

Figure 7. Diffusive and convective components ($\vec{J}_{gD}$, $\vec{J}_{gC}$) of the radon activity flux density, $\vec{J}_g$, averaged along the perimeter of the soil–gap interface, as a function of the applied disturbance pressure difference, Δp.

which is directed toward the gap, changes the mixture of soil gas at the soil–gap interface, altering the value of C_g and at the same time reducing its gradient at the interface. The result then is an increase in the convective component of $\vec{J}_g$ through the gap, accompanied by a decrease in the diffusive component, with a net increase in $\vec{J}_g$. In order to illustrate this behavior, the effect of variable p is explored below. In the next section, the factors affecting the resistance of the flow are analyzed.

The program was run with Δp varying from practically zero to −20 Pa, for three different cases of k equal to 1.0×10^{-13}, 1.0×10^{-12} (base case), and 1.0×10^{-11} m^2. As anticipated, average values of $\vec{q}_g$ at the soil–gap interface were negligible for a very small pressure and increased linearly with Δp, in all three cases.

The variations of C_g/C_g^{∞} at the soil–gap interface as a function of Δp, for the different cases, are shown in Figure 6. Here, for $\Delta p = 0$, the three curves converge to a common finite value reflecting the condition in which the transport of radon is taking place only by molecular diffusion. As Δp increases, the flow of soil gas toward the gap entrance increases and the radon concentration curves respond positively, although with a decreasing slope due to the dilution affect mentioned above. The dilution effect is more evident for the case of high soil permeability ($k = 1.0 \times 10^{-11}$ m^2) in which C_g/C_g^{∞} reaches a maximum at Δp around 5.0 Pa.

Figure 7 shows the variation of the averaged radon activity flux density (its diffusive and convective components), with Δp, for the base case permeability. With no applied disturbance pressure, $\vec{q}_g$ is zero and $\vec{J}_g$ is reduced to its diffusive component, $\vec{J}_{gD}$. As the pressure increases, $\vec{J}_{gD}$ decreases slowly, while the convective component, $\vec{J}_{gC}$, increases very rapidly (almost linearly with pressure). Thus, for the particular configuration of soil permeability, radon diffusion coefficient, and geometry of the base case, the value of $\vec{J}_g$ is dominated by its convective component for applied disturbance pressures above 4.0 Pa. For a larger soil permeability ($k = 1.0 \times 10^{-11}$ m^2), the same pressure range causes a larger variation of $\vec{q}_g$ and the convective component of $\vec{J}_g$ predominates over its diffusive component at applied disturbance pressures higher than 0.4 Pa. The inverse effect was also observed; that is, with $k = 1.0 \times 10^{-13}$ m^2, the convective component predominates only at pressures above 40.0 Pa.

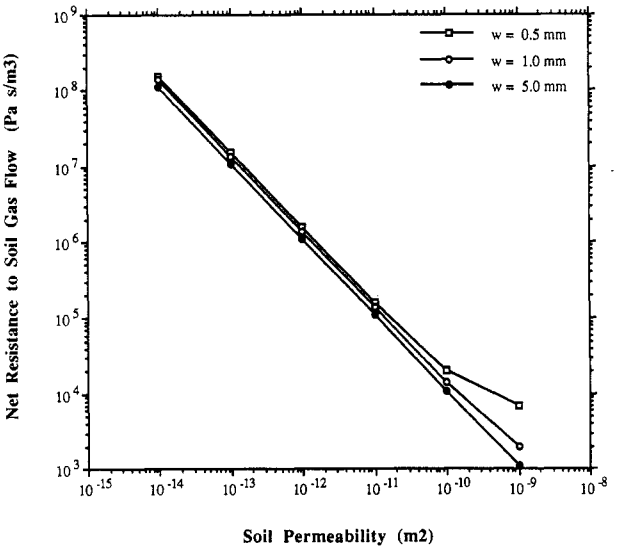

Figure 8. Net resistance to the flow of soil gas, $\mathcal{R}$, as a function of the soil permeability, k, for different values of gap width, w.

Similar to the variation of $\vec{J}_g$, the values of C_{indoor} were also found to respond directly (almost linearly) to Δp. For $\Delta p = 0$, C_{indoor} is equal to 0.54 Bq m^{-3} and independent of k. An increase of Δp from zero to −20.0 Pa, causes an approximate 1.3- 4.8- and 46.0-fold increase in C_{indoor}, for the three cases of k equal to 1.0×10^{-13}, 1.0×10^{-12}, and 1.0×10^{-11} m^2, respectively.

Soil Permeability and Gap Width. The flow of soil gas within the soil and into the house depends on the disturbance pressure distribution in the soil and in the gap, and on the resistance that the soil and gap offer to the transport of the soil gas. The net resistance to the flow of soil gas into the house may be defined as the ratio of the total applied disturbance pressure differential and the average flow of soil gas into the house (Pa s m^{-3}). Both the resistance to the flow and the disturbance pressure field depend on the geometric configuration of the house and the physical properties of the medium, including the gap width, w, and soil permeability, k. In order to investigate the response of the model to variations in w and k, four different values of w were selected: 0.5, 1.0, 5.0, and 10.0 mm. For each of these, the computer model was

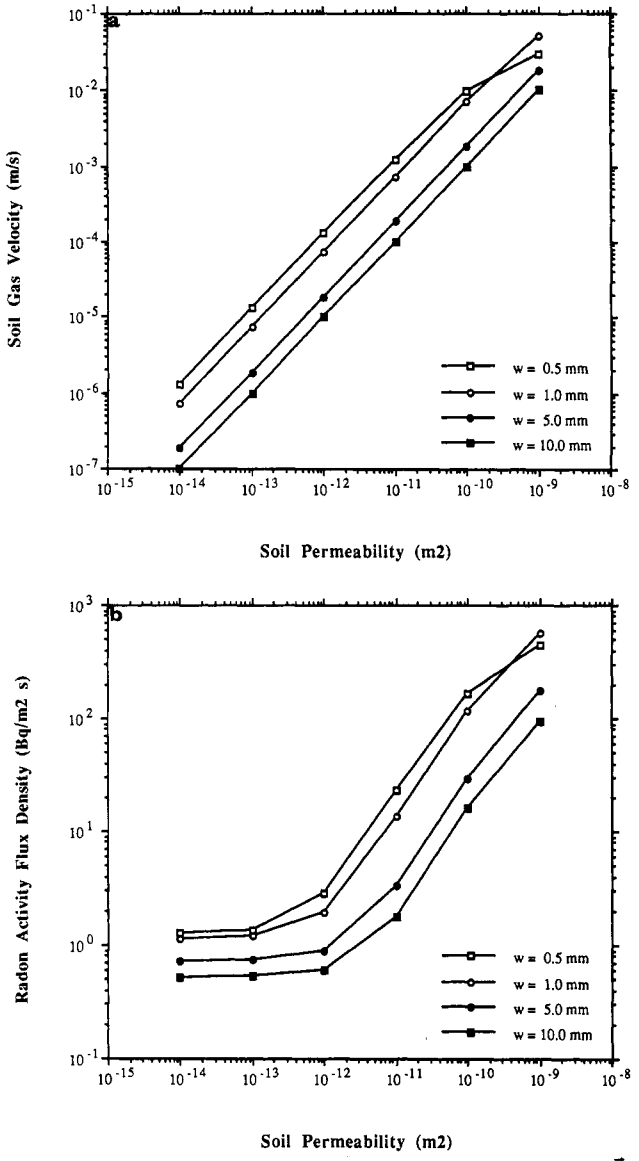

Figure 9. Soil gas velocity, $\vec{q}_g$, and radon activity flux density, $\vec{J}_g$, averaged along the perimeter of the soil–gap interface, as a function of the gap width, w, and soil permeability, k. (a) Soil gas velocity, $\vec{q}_g$, versus soil permeability, k. (b) Radon activity flux density, $\vec{J}_g$, versus soil permeability, k.

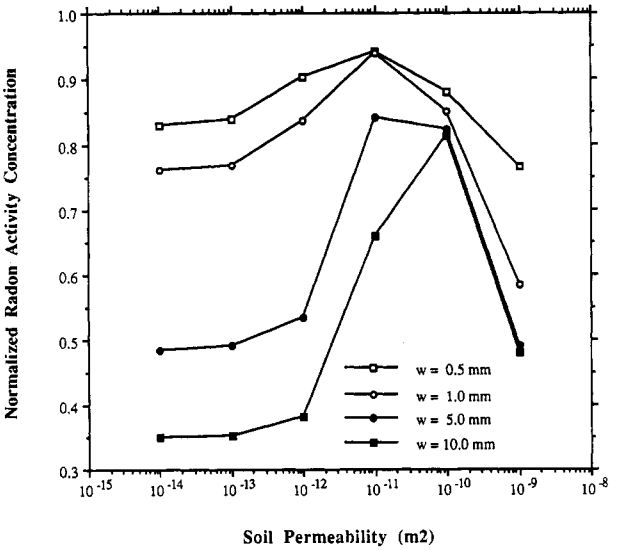

Figure 10. Normalized radon activity concentration in the soil gas, C_g/C_g^{∞}, averaged along the perimeter of the soil–gap interface, as a function of the soil permeability, k, for different values of the gap width, w.

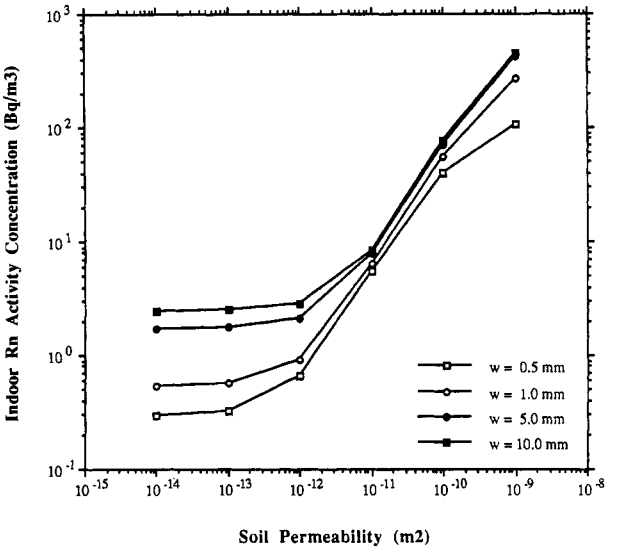

Figure 11. Indoor radon activity concentration, C_{indoor}, as a function of the soil permeability, k, for different values of gap width, w.

run over a range of k from 1.0×10^{-14} to 1.0×10^{-9} m^2. Simulated results are presented in Figures 8–11.

As shown in Figure 8, the net resistance to soil gas flow varies inversely with both w and k. For w larger than 1.0 mm, the net resistance to the soil gas flow varies inversely with k over its whole range of variability. For small gap widths ($w \leq 1.0$ mm), the variation of the net resistance to the soil gas flow is also inversely proportional to k, but now only for k up to 1.0×10^{-11} m^2. Beyond this point, the curves deviate from the original pattern, suggesting a decreasing dependence on k and an increasing dependence on w. These results are consistent with the idea that the net resistance to soil gas flow is composed of a sum of two components: $\mathcal{R}_{soil}$, the soil resistance; and $\mathcal{R}_{gap}$, the gap resistance. By hypothesis, the sum of the pressure drops across the soil and the gap is constant and equal to the total applied disturbance pressure, Δp. However, the pressure drop across each part separately depends on $\mathcal{R}_{gap}$ and $\mathcal{R}_{soil}$ and consequently varies according to the values of k and w. Therefore, the shape of the spatial distribution of the disturbance pressure throughout the soil block, as shown in Figure 4, can be affected by both w and k. For a large gap width ($w > 1.0$ mm), $\mathcal{R}_{gap}$ becomes negligibly small if compared with $\mathcal{R}_{soil}$ and the pressure drop occurs almost entirely within the soil block. In these cases (large w) the disturbance pressure distribution in the soil becomes practically invariable with w and k. On the other hand, for small gap widths ($w \leq 1.0$ mm), $\mathcal{R}_{gap}$ and $\mathcal{R}_{soil}$ can be of comparable magnitude depending on the value of k, and therefore, the disturbance pressure distribution becomes very sensitive to the values of w and k. In such cases, an increase in k causes a reduction of $\mathcal{R}_{soil}$, resulting in an increase of the total flow of soil gas and in a reduction of the pressure drop in he soil block.

We now consider the model's predictions pertaining to the soil gas velocity, $\vec{q}_g$, and the radon activity flux density, $\vec{J}_g$, at the soil–gap interface averaged over the whole gap length. Parts a and b of Figure 9 show the variations of $\vec{q}_g$ and $\vec{J}_g$, respectively, as functions of k, for different values of w. As anticipated, the behavior of $\vec{q}_g$ clearly mimics the observed net resistance behavior shown in Figure 8. In contrast to the soil gas velocity, however, $\vec{J}_g$ does not vary linearly with k over its whole range of variability. This is because $\vec{J}_g$ is a sum of its diffusive and convective com-

ponents, $\vec{J}_{gD}$ and $\vec{J}_{gC}$. Thus, as shown in Figure 9b for k below 1.0×10^{-12} m^2, $\vec{J}_{gD}$ predominates and $\vec{J}_g$ becomes almost invariable with the soil permeability. For k above 1.0×10^{-12} m^2, $\vec{q}_g$ is high, $\vec{J}_{gC}$ predominates, and $\vec{J}_g$ varies almost linearly with k. The variation is not truly linear due to dilution effects on the concentration of radon activity in the soil gas at the gap interface.

It is possible to see in Figure 9 that, for $k = 1.0 \times 10^{-9}$ m^2, an increase in w from 0.5 to 1.0 mm results in an increase of both $\vec{q}_g$ and $\vec{J}_g$, contrary to the general pattern shown in those curves. The explanation for this change in behavior lies in the variation of the net resistance $\mathcal{R}$ to the flow of soil gas for the conditions of very high k and small w. Under these conditions, a change in w by a factor of 2 results in a change in $\mathcal{R}$ by a factor that is larger than the correspondent change in the cross-sectional area of the gap entrance. Consequently both $\vec{q}_g$ and $\vec{J}_g$ increase.

The simulated variations of the normalized radon activity concentration in the soil gas phase, C_g/C_g^∞, at the soil–gap interface, as a function of w and k are shown in Figure 10. For k below 1.0×10^{-12} m^2, C_g varies slowly with k and depends more on w. As k increases above 1.0×10^{-12} m^2, C_g increases to a maximum and then starts to decrease very rapidly. The locations of these concentration peaks depend on w but occur within the range of k between 1.0×10^{-11} and 1.0×10^{-10} m^2. An explanation for this behavior appears to lie in the relative importance of the convective–diffusive flux density components and the lower/upper soil contribution to C_g. For k below 1.0×10^{-12} m^2, $\vec{q}_g$ is small and radon transport occurs mainly by diffusion. Consequently, C_g at the soil–gap interface is almost invariable with soil permeability. As k increases above 1.0×10^{-12} m^2, however, the flow of soil gas toward the gap also increases and C_g becomes highly dependent on k. As the flow of soil gas is increased with k, the profile of C_g throughout the soil block is altered, with the general tendency of moving the isolines of C_g, as seen in Figure 5, closer to the soil–gap interface, altering the overall concentration of radon activity in the soil gas entering the gap channel. This results, then, in a concentration followed by a dilution of C_g at the soil–gap interface as k increased. It should be noted that the observed dilution effect is influenced by the depth of the basement, as well as by the location of the gap in the understructure of the house. Generally, the deeper the basement and the farther the gap is located from the soil surface, the higher C_g will be at the soil–gap interface, under the same conditions.

Finally, the variation of the indoor radon activity concentration, C_{indoor}, with w and k is plotted in Figure 11. Here it is possible to see that C_{indoor} is an increasing function of both w and k. For k below 1.0×10^{-12} m^2, since $\vec{J}_g$ is mainly due to its diffusive component, C_{indoor} varies very slowly with k. But for k above 1.0×10^{-12} m^2, the variation is strongly dependent on the soil permeability, with an almost linear relationship.

Bulk Diffusion Coefficient of Radon in Soil. In the absence of any disturbance pressure in the soil (with no convective flow of soil gas phase), the distribution of C_g with depth is mainly governed by the diffusion coefficient of radon in soil. Under this undisturbed condition, C_g increases exponentially from zero at the soil–air interface, to its maximum finite value at infinite depth in the soil, C_g^∞. The rate at which C_g changes with depth is determined by its *diffusion length* in the soil, representing the distance required for C_g to change by a factor equal to the natural number e. The diffusion length of radon in soil is closely related to its diffusion coefficient. It is defined as $L_D = (D_e/\lambda)^{1/2} = (D/n\lambda)^{1/2}$. For a small D (or a small

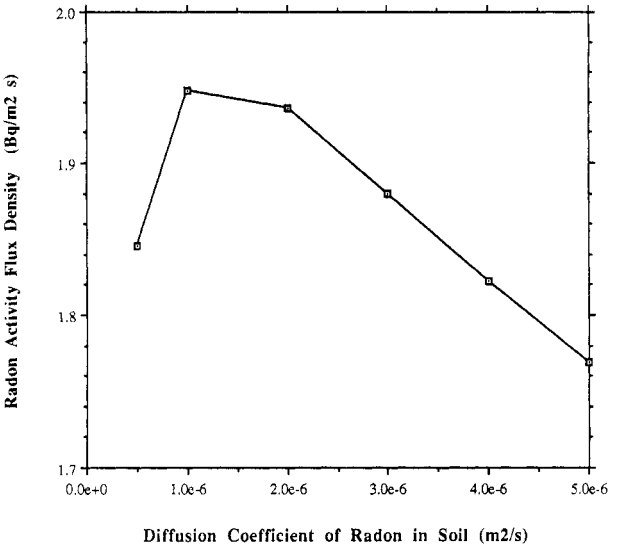

Figure 12. Radon activity flux density, $\vec{J}_g$, averaged along the perimeter of the soil–gap interface, as a function of the bulk diffusion coefficient of radon in soil, D.

diffusion length), C_g reaches its limiting value C_g^∞ at a shallow depth in the soil. The presence of a disturbance pressure distribution in the soil block will tend to alter this natural distribution of C_g with depth. The extent of this alteration will depend on the level of the disturbance pressure, as well as on the values of some physical parameters of the soil (specially the soil permeability) affecting the resistance of the system to the flow of soil gas.

The diffusive component of the radon activity flux density at the soil–gap interface, $\vec{J}_{gD}$, is directly related to D. However, since $\vec{J}_{gC}$ depends upon the distribution of C_g in the soil, which depends in turn upon the diffusion length of radon in soil, D may affect both components ($\vec{J}_{gD}$ and $\vec{J}_{gC}$) of the radon activity flux density into the house. Figure 12 illustrates the sensitivity of the model to the bulk radon diffusion coefficient in soil. As D increases from 0.5×10^{-6} to 1.0×10^{-6} m^2 s^{-1}, the absolute value of $\vec{J}_g$ at the gap also increases. With a further increase in D above 1.0×10^{-6} m^2 s^{-1}, the variation of $\vec{J}_g$ is reversed, showing an inverse correlation with the D. For a small D on the order of 0.5×10^{-6} m^2 s^{-1}, the diffusion length is relatively small. This means that the vertical profile of C_g reaches its limit value at a shallow depth. Consequently, at the depth in the soil where the gap is located, C_g is already near its limit value, and the diffusion of radon into the gap is not affected by the presence of the air–soil interface at the upper part of the soil block. In such cases, the concentration of radon activity at the soil–gap interface increases with D, resulting in an increase of both the diffusive and convective components of $\vec{J}_g$, as indicated in the first part of the curve in Figure 12. As the diffusion length increases, however, the vertical profile of C_g in the soil is altered, reducing the concentration at the level where the gap is located. In such cases, $\vec{J}_{gD}$ increases while $\vec{J}_{gC}$ decreases due to the reduction in the radon activity concentration in the soil gas around the gap. Consequently, the net variation of $\vec{J}_g$ is the result of these two distinct tendencies. As shown in Figure 12, the absolute value of $\vec{J}_g$ decreased slightly, with a doubling of D from 1×10^{-6} to 2×10^{-6} m^2 s^{-1}, but beyond this point $\vec{J}_g$ decreased rapidly with an increase in D.

Soil Porosity. According to eq 9, the production rate of radon into the soil pore space is inversely related to the effective porosity, n, of the soil. Thus, to test the response of the computer model to variations of the soil porosity, the model was run with n varying from 0.2 to 0.6. The

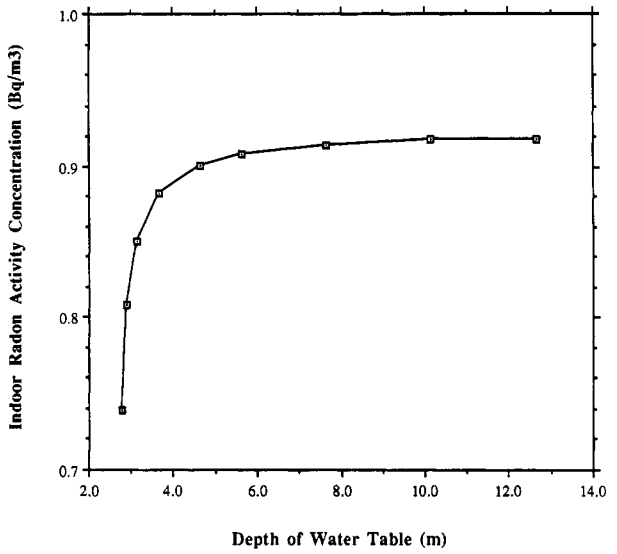

Figure 13. Indoor radon activity concentration, C_{indoor}, as a function of the water table depth, z_{WT}.

simulated results indicate that the model is quite sensitive to n. For example, variation of n from 0.4 to 0.6, causes an approximate decrease in $\bar{J}_g$ and C_{indoor} by a factor of 2. It may be misleading to vary porosity independently, however. In reality, variation in soil porosity would generally imply a variation in other soil parameters, such as the soil permeability and diffusion coefficient, which would affect radon transport in the manner discussed above.

Depth of Water Table. A layer of unsaturated soil extending 10.50 m below the basement slab (d_{WT} = 12.65 m from the soil surface) was adopted for the characterization of the base case described herein. Although justifiable under our assumptions regarding a dry soil application of the model, it is recognized that an unsaturated zone of that size is not common in many localities. Therefore, to conclude our analysis, the model was tested for the effect of varying the depth of the water table, d_{WT}, from a distance of 0.125 m underneath the basement slab (d_{WT} = 2.275 m from the soil surface) to the original depth adopted in the base case. The simulated results representing the variation of C_{indoor} with d_{WT} are shown in Figure 13. The presence of a saturated zone at a shallow depth in the soil tends to reduce the volume of soil contributing to the generation of radon into the soil gas phase, thereby reducing its availability to enter the house. The value of C_{indoor} at d_{WT} = 2.275 is about 80.0% of its value at d_{WT} = 12.65 m. It is important to note that most of this variation takes place in the range of d_{WT} between 2.275 and 5.0 m. For $d_{WT} > 5.0$ m, C_{indoor} is practically unaffected by the value of the water table depth. Thus, the simulated results presented herein would not be altered significantly if we had adopted, for the base case, a water table depth with $d_{WT} \geq 5.0$ m.

Summary and Conclusions

Among the variables analyzed herein, those that were shown to have the most dramatic effect on the behavior of the model are the following: the concentration of radium in the soil, the soil permeability, and the applied disturbance pressure. The radon source variables controlling radon production in the soil (such as the ^{226}Ra concentration in soil particles, and the radon emanation fraction) are very significant to the availability and transport of radon through the soil and into houses. A direct linear relation exists between these variables and the indoor radon concentration. The applied disturbance pressure in the basement was also shown to be have a direct, though not linear, effect on the model's predictions. Becuase of its large range of variability, the soil permeability appears to have the greatest effect on the process of radon transport through the soil and its entrance into houses. For the conditions established for the base case, a turning point of $k = 1.0 \times 10^{-12}$ m^2 (representative of a fine sand or silty soil) has been predicted in the diffusive–convective characterization of radon transport in the soil gas. For clayey soils with permeabilities below that value, the velocity of the soil gas is relatively small, and the transport of radon through the soil into the house becomes diffusive controlled. Under these circumstances, the flow of radon into the house and the resultant indoor radon concentration would be essentially independent of the soil permeability, being affected predominantly by the source-related variables. For soil permeabilities above that level, the transport of radon becomes dominated by the convective movement of the soil gas, resulting in a direct (almost linear) dependence of the indoor radon concentration on soil permeability. It should be emphasized, though, that this turning point value of 1.0×10^{-12} m^2 for the soil permeability is inversely dependent on the applied disturbance pressure.

The simulated results presented herein have shown that the model performs consistently with physical expectations. However, validation of the model must be undertaken before more definitive conclusions can be drawn from this analysis. Model validation is presently in progress through the Indoor Environment Program, Lawrence Berkeley Laboratory, where simulations are being compared with measured data from family houses. After validation, the model could be used for the investigation of other specific scenarios and in helping to design new experiments. For example, our present simulations have indicated that the concentration of radon in the soil gas entering the house is dramatically affected by the geometry of the house, the applied disturbance pressure, and the soil permeability. Thus, the model could be used to simulate the effectiveness of employing low radium graded materials in the aggregate regions around the basement. The objective would be to minimize radon entrance into the house by decreasing the radon availability in the region of the soil near the gap entrance, blocking the passage of radon-rich soil gas from deep in the soil, and enhancing the dilution effect caused by radon-poor soil gas from the upper part of the soil block. The results from simulations of this kind could help determine the best range of parameters to optimize the control of indoor radon concentrations in new houses.

Improvements of the model can be identified to extend its range of applicability to more general cases. In this regard, a model option could be developed to define other openings at arbitrary locations in the building understructure. Also, the effect of soil moisture and temperature variation on the generation and transport of radon, within the unsaturated zone of the subsurface soil, could be incorporated. To improve model flexibility, the applied disturbance pressure and the air exchange rate in the house could be treated as a function of the disturbance pressure generating mechanisms such as wind speed, temperature differences, and unbalanced mechanical ventilation.

Registry No. ^{222}Rn, 14859-67-7; ^{226}Ra, 13982-63-3.

Literature Cited

(1) Nero, A. V. *Health Phys.* **1983**, *45*, 303.
(2) Nero, A. V.; Nazaroff, W. W. *Radiat. Prot. Dosim.* **1984**, *7*, 23.

(3) Nero, A. V. In *Radon and Its Decay Products in Indoor Air*; Nazaroff, W. W., Nero, A. V., Eds.; Wiley: New York, 1988; Chapter 1.
(4) Sextro, R. G.; Moed, B. A.; Nazaroff, W. W.; Revzan, K. L.; Nero, A. V. In *Radon and Its Decay Products: Occurrences, Properties, and Health Effects*; Hopke, P., Ed.; ACS Symposium Series 331; American Chemical Society: Washington, DC, 1987; Chapter 2.
(5) The Effects on Populations of Exposure to Low Levels of Ionizing Radiation. BEIR III Report; Committee on the Biological Effects of Ionizing Radiations, National Academy Press: Washington, DC, 1980.
(6) Ionizing Radiation: Sources and Biological Effects. UNSCEAR Report to the General Assembly, United Nations: New York, 1982.
(7) Exposures from the Uranium Series with Emphasis on Radon and its Daughters. NCRP Report No. 77; National Council on Radiation Protection and Measurements: Bethesda, MD, 1984.
(8) Evaluation of Occupational and Environmental Exposures to Radon and Radon Daughters in the United States. NCRP Report No. 78; National Council on Radiation Protection and Measurements: Bethesda, MD, 1984.
(9) Tanner, A. B. In *The Natural Radiation Environment*; Adams, J. A. S., Lowder, W. M., Eds.; University of Chicago Press: Chicago, IL, 1964; p 161.
(10) Tanner, A. B. In *Proceedings, Natural Radiation Environment III*; Gessel, T. S., Lowder, W. M., Eds.; Conf-780422; U.S. Department of Commerce, National Technical Information Service: Springfield, VA, 1980; p 5.
(11) Clements, W. E. The Effect of Atmospheric Pressure Variation on the Transport of Rn-222 from the Soil to the Atmosphere. Ph.D. Dissertation, New Mexico Institute of Mining and Technology, Socorro, NM, 1974.
(12) Clements, W. E.; Wilkening, M. H. *J. Geophys. Res.* **1974**, *79*, 5025.
(13) Rogers, V. C.; Nielson, K. K. *A Handbook for the Determination of Radon Attenuation Through Cover Materials*; NUREG/CR-2340. U.S. Nuclear Regulatory Commission: Bethesda, MD, 1981.
(14) Rogers, V. C.; Nielson, K. K.; Merrell, G. B.; Kalkwarf, D. R. *The Effects of Advection on Radon Transport Through Earthen Materials*; NUREG/CR-2309; U.S. Nuclear Regulatory *Commission*: Bethesda, MD, 1983.
(15) Bates, R. C.; Edwards, J. C. In *Proceedings of the International Mine Ventilation Congress*; Society of Mining Engineers: New York, 1980; p 412.
(16) Edwards, J. C.; Bates, R. C. *Health Phys.* **1980**, *39*, 263.
(17) Bates, R. C.; Edwards, J. C. In *Radiation Hazard in Mining: Control, Measurement, and Medical Aspects*; Gomes, M., Ed.; Society of Mining Engineers: New York, 1981; p 149.
(18) Collé, R.; Rubin, R. J.; Knab, L. T.; Hutchinson, J. M. R. *Radon Transport Through and Exhalation from Building Materials: A Review and Assessment*; NBS Technical Note 1139; U.S. Department of Commerce, National Bureau of Standards: Washington, DC, 1981.
(19) Bruno, R. C. *J. Air Pollut. Control Assoc.* **1983**, *33*, 105.
(20) Åkerblom, G.; Anderson, P.; Clavensjö, B. *Radiat. Prot. Dosim.* **1984**, *7*, 49.
(21) Nazaroff, W. W.; Moed, B. A.; Sextro, R. G. In *Radon and Its Decay Products in Indoor Air*; Nazaroff, W. W., Nero, A. V., Eds.; Wiley: New York, 1988; Chapter 2.
(22) Mowris, R. J. Analytical and Numerical Models for Estimating the Effect of Exhaust Ventilation on Radon Entry in Houses with Basements or Crawl Spaces. LBL-22067; M.S. Thesis, Lawrence Berkeley Laboratory, Berkeley, CA, 1986.
(23) Mowris, R. J.; Fisk, W. J. *Health Phys.* **1988**, *54*, 491.
(24) Nazaroff, W. W.; Sextro, R. G. *Environ. Sci. Technol.* **1989**, *23*, 451.
(25) Scott, A. G. Computer Modeling of Radon Movement. In *EML Indoor Radon Workshop*; Report EML-416; George, A. C., Lowder, W., Fisenne, I., Knutson, E. O., Hinchcliffe, L., Eds.; Environmental Measurements Laboratory: New York, 1982.
(26) DSMA Atcon Ltd. Review of Existing Instrumentation and Evaluation of Possibilities for Research and Development of Instrumentation to Determine Future Levels of Radon at a Proposed Building Site. INFO-0096; Report to the Atomic Energy Control Board, Ottawa, Ontario, Canada, 1983.
(27) Eaton, R. S.; Scott, A. G. *Radiat. Prot. Dosim.* **1984**, *7*, 251.
(28) DSMA Atcon Ltd. A Computer Study of Soil Gas Movement into Basements. Report 1389/1333; Report to the Department of Health and Welfare, Ottawa, Ontario, Canada, 1985.
(29) *FY-1988 Radon Research Program.* DOE/ER-0405; U.S. Department of Energy, Office of Energy Research, Office of Health and Environmental Research: Washington, DC, 1989.
(30) Loureiro, C. de O. Simulation of the Steady-State Transport of Radon from Soil into Houses with Basements under Constant Negative Pressure. LBL-24378; Ph.D. Dissertation, Lawrence Berkeley Laboratory, Berkeley, CA, 1987.
(31) Tanner, A. B. *Radiat. Prot. Dosim.* **1988**, *24*, 79.
(32) Garbesi, K.; Sextro, R. G. *Environ. Sci. Technol.* **1989**, *23*, 1481.
(33) Holford, D. J.; Gee, G. W.; Owczarski, P. C.; Freeman, H. D. A Finite-Element Model of Radon Advection and Diffusion in Unsaturated Cracked Soils. Presented at the American Geophysical Union, Fall Meeting, San Francisco, CA, 1988.
(34) Owczarski, P. C.; Holford, D. C.; Freeman, H. D.; Gee, G. W. Effect of Soil Porosity, Permeability, and Water Content on Radon Flux from Soil Surfaces. Presented at the American Geophysical Union, Spring Meeting, Baltimore, MD, 1989.
(35) Nielson, K. K.; Rogers, V. C. Radon Generation, Absorption and Transport in Porous Media—the RAETRAN Model. Presented at the American Geophysical Union, Spring Meeting, Baltimore, MD, 1989.
(36) Abriola, L. M. *Multiphase Flow and Transport Models for Organic Chemicals: A Review and Assessment*; EPRI EA-5976; Electric Power Research Institute: Palo Alto, CA, 1988.
(37) Bear, J. *Dynamics of Fluids in Porous Media, 1st ed.*; Dover Publications, Inc.: Mineola, NY, 1988.
(38) Weast, R. C., Astle, M. J., Beyer, W. H., Eds. *CRC Handbook of Chemistry and Physics*, 68th ed.; CRC Press, Inc.: Boca Raton, FL, 1988; p F.44.
(39) Patankar, S. V. *Numerical Heat Transfer and Fluid Flow*, 1st ed.; McGraw-Hill Book Co.: New York, 1980.
(40) Anderson, D. A.; Tannerhi, J. C.; Pletcher, R. H. *Computational Fluid Mechanics and Heat Flow*, 1st ed.; McGraw-Hill Book Co.: New York, 1984.
(41) Schiller, G. E. A Theoretical Convective-Transport Model of Indoor Radon Decay Products. Ph.D. Dissertation, University of California, Berkeley, CA, 1984.

Received for review August 14, 1989. Revised manuscript received April 13, 1990. Accepted April 16, 1990. This work was made possible with a research assistantship provided by the Indoor Environment Program, at Lawrence Berkeley Laboratory, and supported by the U.S. Department of Energy through Contract No. DE-AC03-76SF00098.